

Highlights

FPDIoU Loss: A Loss Function for Efficient Bounding Box Regression of Rotated Object Detection

Siliang Ma, Yong Xu

- Bounding box regression is a significant process of rotated object detection.
- Most of the existing loss functions for rotated object detection are extremely complex or with low efficiency.
- Geometrical properties are not fully considered to design the losses of bounding box regression.
- We proposed \mathcal{L}_{FPDIoU} based on four points distance to tackle the issues of existing losses and with higher efficiency and accuracy.

FPDIoU Loss: A Loss Function for Efficient Bounding Box Regression of Rotated Object Detection

Siliang Ma^a, Yong Xu^{a,b,*}

^aInstitute of Computer Science and Engineering, South China University of Technology, No. 382, Outer Ring East Road, Panyu District, Guangzhou, 510006, Guangdong, China

^bPengcheng Laboratory, No. 2, Xingke 1st Street, Nanshan District, Shenzhen, 518000, Guangdong, China

ARTICLE INFO

Keywords:

Rotated object detection
bounding box regression
loss function
minimum points distance

ABSTRACT

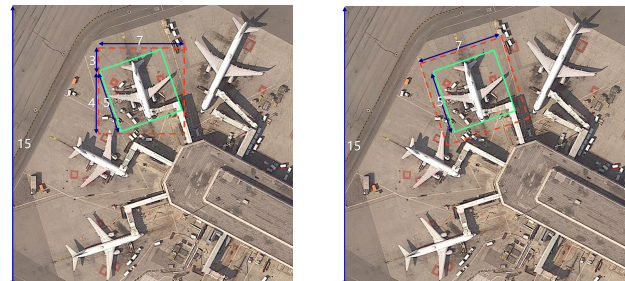
Bounding box regression is one of the important steps of object detection. However, rotation detectors often involve a more complicated loss based on SkewIoU which is unfriendly to gradient-based training. Most of the existing loss functions for rotated object detection calculate the difference between two bounding boxes only focus on the deviation of area or each points distance (e.g., $\mathcal{L}_{Smooth-\ell_1}$, $\mathcal{L}_{RotatedIoU}$ and \mathcal{L}_{PIoU}). The calculation process of some loss functions is extremely complex (e.g. \mathcal{L}_{KFIoU}). In order to improve the efficiency and accuracy of bounding box regression for rotated object detection, we proposed a novel metric for arbitrary shapes comparison based on minimum points distance, which takes most of the factors from existing loss functions for rotated object detection into account, i.e., the overlap or nonoverlapping area, the central points distance and the rotation angle. We also proposed a loss function called \mathcal{L}_{FPDIoU} based on four points distance for accurate bounding box regression focusing on faster and high quality anchor boxes. In the experiments, $FPDIoU$ loss has been applied to state-of-the-art rotated object detection (e.g., RTMDET, H2RBox) models training with three popular benchmarks of rotated object detection including DOTA, DIOR, HRSC2016 and two benchmarks of arbitrary orientation scene text detection including ICDAR 2017 RRC-MLT and ICDAR 2019 RRC-MLT, which achieves better performance than existing loss functions.

1. Introduction

Rotated object detection can be considered as a special circumstance of object detection, which has attracted a large scale of researchers' interests during the past few years. Most of the state-of-the-art rotated object detectors can be modified based on horizontal object detectors (e.g., YOLO series [1–6], Faster R-CNN [7], reppoints [8] and retinanet [9]), which rely on a bounding box regression (BBR) module to localize objects.

During the past few years, IoU [10] has been widely used for comparing the similarity between two arbitrary shapes based on the overlap area. This property makes IoU invariant to the scale of the problem under consideration. Due to this appealing property, most of the performance measures used to evaluate for instance segmentation [11–14], object detection [12, 15], and tracking [16] rely on this metric.

However, as Figure 1 shows, most of the existing loss functions for bounding box regression have the same value in some special cases, which will limit the convergence speed and accuracy. Therefore, we try to design a novel loss function called \mathcal{L}_{FPDIoU} for bounding box regression with consideration of the advantages included in $\mathcal{L}_{RotatedIoU}$, \mathcal{L}_{GIoU} , \mathcal{L}_{DIOU} , \mathcal{L}_{PIoU} and \mathcal{L}_{KFIoU} , but also has higher efficiency and accuracy for bounding box regression.



(a) $\mathcal{L}_{RotatedIoU} = 0.4898$,
 $\mathcal{L}_{GIoU} = 0.4898$,
 $\mathcal{L}_{DIOU} = 0.4898$,
 $\mathcal{L}_{PIoU} = 0.4898$,
 $\mathcal{L}_{KFIoU} = 3.6563$,
 $\mathcal{L}_{FPDIoU} = 0.5296$

(b) $\mathcal{L}_{RotatedIoU} = 0.4898$,
 $\mathcal{L}_{GIoU} = 0.4898$,
 $\mathcal{L}_{DIOU} = 0.4898$,
 $\mathcal{L}_{PIoU} = 0.4898$,
 $\mathcal{L}_{KFIoU} = 3.6563$,
 $\mathcal{L}_{FPDIoU} = 0.4986$

Figure 1: Two cases with different bounding boxes regression results. The green boxes denote the groundtruth bounding boxes and the red boxes denote the predicted bounding boxes. The $\mathcal{L}_{RotatedIoU}$, \mathcal{L}_{GIoU} , \mathcal{L}_{DIOU} , \mathcal{L}_{PIoU} , \mathcal{L}_{KFIoU} between these two cases are exactly same value, but their \mathcal{L}_{FPDIoU} values are very different.

In this paper, we will address the issues of the existing IoU -based metrics by considering the mathematical definition of rotated rectangle. We ensure this novel metric for bounding box regression follows the same definition as IoU , i.e. encoding the shape properties of the compared objects into the region property. In addition, it is valid whether the predicted bounding box and the groundtruth bounding box are overlap or not. We introduce this IoU based on

*Corresponding author

✉ 1 (S. Ma); 2 (Y. Xu)

✉ 202010107394@mail.scut.edu.cn (S. Ma); yxu@scut.edu.cn (Y. Xu)

ORCID(s): 0000-0001-7117-9333 (S. Ma)

four points distance, named $FPDIoU$, as a new metric for comparing any two arbitrary shapes. We also provide an analytical solution for calculating $FPDIoU$ between two rotated rectangles, allowing it to be used as a loss in this case. Incorporating $FPDIoU$ loss into state-of-the-art rotated object detection algorithms, we consistently improve their performance on popular object detection benchmarks such as DOTA [17], DIOR [18] and HRSC2016 [19] and arbitrary orientation scene text spotting benchmarks ICDAR 2017 RRC-MLT [20] and ICDAR 2019 RRC-MLT [21] using the standard evaluation metric, i.e. IoU based [12, 15] performance measure.

The contributions of this paper can be summarized as below:

1. We considered the advantages and disadvantages of the existing IoU -based losses and ℓ_n -norm losses, we propose an IoU loss based on four points distance called \mathcal{L}_{FPDIoU} to tackle the issues of existing losses and obtain a faster convergence speed and more accurate regression results.
2. Extensive experiments have been conducted on rotated object detection tasks. We compared with the existing loss functions for rotated bounding box regression and the SOTA rotated object detectors. Outstanding experimental results validate the superiority of the proposed $FPDIoU$ loss.

2. Related Work

2.1. Rotated Object Detection

Different from horizontal object detection, rotated object detection needs to consider not only the central points, width and height of the bounding boxes, but also the rotation angle. At the very beginning, researchers attempted to extend classical horizontal detectors [7, 22, 23] to the rotation case by adopting the rotated bounding boxes. As we all know, aerial images and arbitrary orientation scene text spotting are popular application of rotated object detection. For aerial images, objects are always not with large aspect ratios. To this end, various rotated object detection models have been proposed. As for single stage methods, DRN [24], DAL [25], R³Det [26], RSDet and S²A-Net [27] are widely used to deal with rotated object detection tasks. While ICN [28], ROI-Transformer [29], SCRDet [30], Mask OBB [31], Gliding Vertex [32], ReDet [33] are two-stage mainstreamed approaches whose pipeline is inherited from Faster RCNN [7]. In order to provide more efficient and accurate rotated object detection results, RTMDET [34] was proposed to deal with real-time rotated object detection tasks, which uses dynamic soft labels to optimize training strategies. However, in order to simplify the rotated object detection problem, a weakly supervised method named H2RBox [35] was proposed which only use horizontal annotations to deal with rotated object detection task. No matter we choose which rotated object detectors, the bounding box regression is necessary, which performs significant role in rotated object detection.

2.2. Variants of IoU-based Loss

It is well-known that IoU -based losses have been widely used in horizontal object detection. At the very beginning,

\mathcal{L}_n -norm loss function was widely used for bounding box regression, which was exactly simple but sensitive to various scales. In YOLO v1 [36], square roots for w and h are adopted to mitigate this effect, while YOLO v3 [2] uses $2 - wh$. In order to better calculate the diverse between the groundtruth and the predicted bounding boxes, IoU loss is used since Unitbox [37]. To ensure the training stability, Bounded- IoU loss [38] introduces the upper bound of IoU . The original IoU can be formulated as

$$RotatedIoU = \frac{\mathcal{B}_{gt} \cap \mathcal{B}_{prd}}{\mathcal{B}_{gt} \cup \mathcal{B}_{prd}}, \quad (1)$$

where \mathcal{B}_{gt} denotes the groundtruth bounding box, \mathcal{B}_{prd} denotes the predicted bounding box. As we can see, the $RotatedIoU$ only calculates the union area of two bounding boxes, which can't distinguish the cases that two boxes do not overlap. If the predicted bounding box completely covers the groundtruth bounding box, the IoU value will not change regardless of the rotation angle.

As equation 1 shows, if $|\mathcal{B}_{gt} \cap \mathcal{B}_{prd}| = 0$, then $IoU(\mathcal{B}_{gt}, \mathcal{B}_{prd}) = 0$. In this case, IoU can not reflect if two shapes are in vicinity of each other or very far from each other. Then, $GIoU$ [39] is proposed to tackle this issue. The $GIoU$ can be formulated as

$$GIoU = RotatedIoU - \frac{|C - \mathcal{B}_{gt} \cup \mathcal{B}_{prd}|}{|C|}, \quad (2)$$

where C is the smallest box covering \mathcal{B}_{gt} and \mathcal{B}_{prd} , and $|C|$ is the area of box C . Due to the introduction of the penalty term in $GIoU$ loss, the predicted box will move toward the target box in nonoverlapping cases. $GIoU$ loss has been applied to train state-of-the-art object detectors, such as YOLO v3 and Faster R-CNN, and achieves better performance than MSE loss and IoU loss. However, $GIoU$ will lost effectiveness when the predicted bounding box is absolutely covered by the groundtruth bounding box. In order to deal with this problem, $DIoU$ [40] was proposed with consideration of the centroid points distance between the predicted bounding box and the groundtruth bounding box. The formulation of $DIoU$ can be formulated as

$$DIoU = RotatedIoU - \frac{\rho^2(\mathcal{B}_{gt}, \mathcal{B}_{prd})}{C^2}, \quad (3)$$

where ρ denotes Euclidean distance. As we can see, the target of \mathcal{L}_{DIoU} directly minimizes the distance between central points of predicted bounding box and groundtruth bounding box. However, when the central point of predicted bounding box coincides with the central point of groundtruth bounding box, it degrades to the original IoU . To address this issue, $CIoU$ was proposed with consideration of both central points distance and the aspect ratio. The formulation of $CIoU$ can be written as follows:

$$CIoU = RotatedIoU - \frac{\rho^2(\mathcal{B}_{gt}, \mathcal{B}_{prd})}{C^2} - \alpha V, \quad (4)$$

$$V = \frac{4}{\pi^2} (\arctan \frac{w^{gt}}{h^{gt}} - \arctan \frac{w^{prd}}{h^{prd}})^2, \quad (5)$$

$$\alpha = \frac{V}{1 - IoU + V}. \quad (6)$$

However, the definition of aspect ratio from $CIoU$ is relative value rather than absolute value, which is not that accurate for bounding box regression. To address this issue, $EIoU$ [41] was proposed based on $DIoU$, which is defined as follows:

$$EIoU = DIoU - \frac{\rho^2(w_{prd}, w_{gt})}{(w^c)^2} - \frac{\rho^2(h_{prd}, h_{gt})}{(h^c)^2}. \quad (7)$$

According to our survey, $CIoU$ and $EIoU$ are not widely used in rotated object detection because the distance between two not parallel lines is difficult to calculate. In order to calculate the IoU more accurately, $PIoU$ [42] was proposed based on pixel-level area calculation. The keypoint of $PIoU$ is how to judge a pixel is inside or outside the predicted bounding box and groundtruth bounding box. The formula is shown as below:

$$\delta(p_{i,j}|b) = \begin{cases} 1, & d_{i,j}^w \leq \frac{w}{2}, d_{i,j}^h \leq \frac{h}{2} \\ 0, & otherwise. \end{cases} \quad (8)$$

where $d_{i,j}$ denotes the Euclidean distance between pixel (i, j) and central point (c_x, c_y) of predicted bounding box or groundtruth bounding box, d_w and d_h denote the distance d along horizontal and vertical direction respectively:

$$d_{i,j} = \sqrt{(c_x - i)^2 + (c_y - j)^2}, \quad (9)$$

$$d_{i,j}^w = |d_{i,j} \cos \beta|, \quad (10)$$

$$d_{i,j}^h = |d_{i,j} \sin \beta|, \quad (11)$$

$$\beta = \begin{cases} \theta + \arccos \frac{c_x - i}{d_{ij}}, & c_y - j \geq 0 \\ \theta - \arccos \frac{c_x - i}{d_{ij}}, & c_y - j < 0 \end{cases}. \quad (12)$$

To ensure the $PIoU$ as a continuous and differentiable function, the definition of $PIoU$ is shown as below:

$$K(d, s) = 1 - \frac{1}{1 + e^{-k(d-s)}}, \quad (13)$$

$$F(p_{i,j}|b) = K(d_{i,j}^w, w) * K(d_{i,j}^h, h), \quad (14)$$

where k is an adjustable factor to control the sensitivity of the target pixel $p_{i,j}$. To reduce the calculational complexity The intersection area $S_{B_{gt} \cap B_{prd}}$ and union area $S_{B_{gt} \cup B_{prd}}$ between B_{gt} and B_{prd} can be approximately defined as:

$$S_{B_{gt} \cap B_{prd}} \approx \sum_{p_{i,j} \in B_{gt}, B_{prd}} F(p_{i,j}|B_{gt})F(p_{i,j}|B_{prd}), \quad (15)$$

$$S_{B_{gt} \cup B_{prd}} \approx \sum_{p_{i,j} \in B_{gt}, B_{prd}} F(p_{i,j}|B_{gt}) + F(p_{i,j}|B_{prd}) - F(p_{i,j}|B_{gt})F(p_{i,j}|B_{prd}), \quad (16)$$

$$PIoU = \frac{S_{B_{gt} \cap B_{prd}}}{S_{B_{gt} \cup B_{prd}}}. \quad (17)$$

On the other hand, some researchers start to think about how to make full use of Gaussian modeling. GWD[43] was proposed based on Gaussian Wasserstein Distance which leads to an approximate and differentiable IoU induced loss. The calculation process of GWD is formulated as:

$$\begin{aligned} d^2 &= \|m_1 - m_2\|_2^2 + \|\Sigma_1^{\frac{1}{2}} - \Sigma_2^{\frac{1}{2}}\|_F^2 \\ &= (x_1 - x_2)^2 + (y_1 - y_2)^2 + \frac{(w_1 - w_2)^2 + (h_1 - h_2)^2}{4} \\ &= \ell_2 - \text{norm}([x_1, y_1, \frac{w_1}{2}, \frac{h_1}{2}]^T, [x_2, y_2, \frac{w_2}{2}, \frac{h_2}{2}]^T) \end{aligned} \quad (18)$$

$$GWD = \frac{1}{\tau + f(d^2)}, \tau \geq 1 \quad (19)$$

where $f(\cdot)$ denotes a non-linear function to transform the Wasserstein distance d^2 to make the loss more smooth and expressive. The hyperparameter τ modulates the GWD. Although GWD scheme has played a preliminary exploration of the deductive paradigm, it does not focus on achieving high-precision detection and scale invariance. Similar with GWD, KLD [44] was proposed with a better central point optimization mechanism, which also transforms the rotated rectangle to the 2-D Gaussian distribution. The KLD between two 2-D Gaussian can be formulated as:

$$D_{kl}(\mathcal{N}_p \| \mathcal{N}_t) = \frac{1}{2}(\mu_p - \mu_t)^T \Sigma_t^{-1}(\mu_p - \mu_t) + \frac{1}{2}Tr(\Sigma_t^{-1} \Sigma_p) + \frac{1}{2} \ln \frac{|\Sigma_t|}{|\Sigma_p|} - 1 \quad (20)$$

$D_{kl}(\mathcal{N}_p \| \mathcal{N}_t)$ is composed of partial parameter coupling, which makes all parameters form a chain coupling relationship. In the optimization process of the KLD-based detector, the parameters can influence each other and are jointly optimized, which leads to the optimization mechanism of the model self-modulated. To make full use of the advantages of Gaussian modeling, KFIOU [45] was proposed based on Gaussian distribution. The volume of a specific rotated bounding box can be formulated as:

$$v_B(\Sigma) = 2^n \sqrt{|\text{eig}(\Sigma)|} = 2^n |\Sigma^{\frac{1}{2}}| = 2^n |\Sigma|^{\frac{1}{2}}, \quad (21)$$

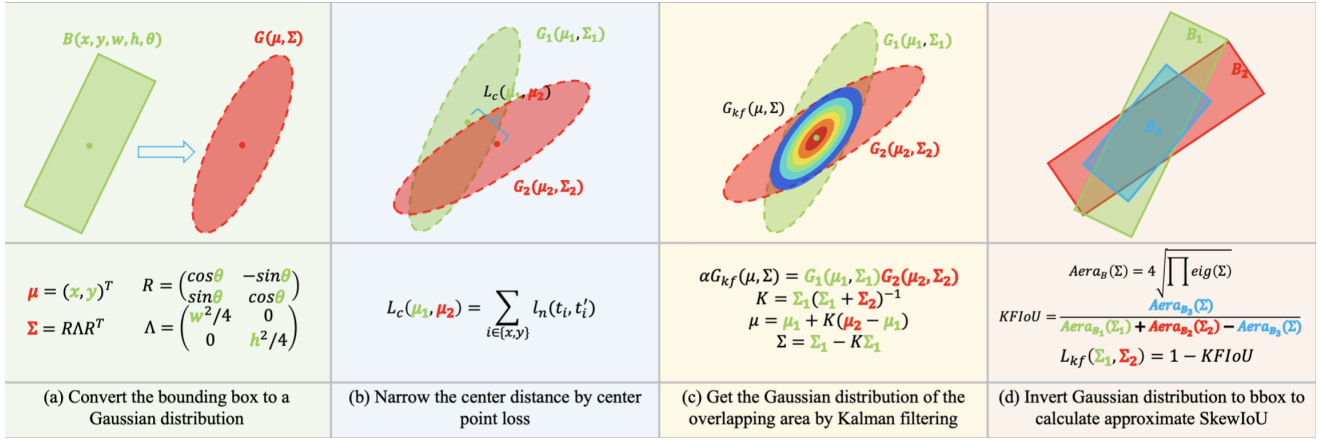


Figure 2: SkewIoU loss approximation process in two-dimensional space based on Gaussian product. Compared with GWD loss [43] and KLD loss [44], our approach follows the calculation process of SkewIoU without introducing additional hyperparameters. We believe such a design is more mathematically rigorous and more in line with SkewIoU loss

where n denotes the number of dimensions. The distribution function of the overlapping area of two Gaussian distributions $\mathcal{N}_x(\mu_1, \Sigma_1)$ and $\mathcal{N}_x(\mu_2, \Sigma_2)$ can be formulated as:

$$\alpha \mathcal{N}_x(\mu, \Sigma) = \mathcal{N}_x(\mu_1, \Sigma_1) \mathcal{N}_x(\mu_2, \Sigma_2), \quad (22)$$

$$\alpha = \mathcal{N}_{\mu_1}(\mu_2, \Sigma_1 + \Sigma_2), \quad (23)$$

where $\mu = \mu_1 + K(\mu_2 - \mu_1)$, $\Sigma = \Sigma_1 - K\Sigma_1$, and K is the Kalman gain, $K = \Sigma_1(\Sigma_1 + \Sigma_2)^{-1}$. To minimize the deviation of two rotated bounding box, we use a center point loss \mathcal{L}_c to narrow the distance between the center of the two Gaussian distributions. In this way, α can be approximated as a constant, and the introduction of the \mathcal{L}_c also allows the entire loss to continue to optimize the detector in non-overlapping cases. The overlap area can be calculated as follows:

$$KFIoU = \frac{\mathcal{V}_{B_3}(\Sigma)}{\mathcal{V}_{B_1}(\Sigma_1) + \mathcal{V}_{B_2}(\Sigma_2) - \mathcal{V}_{B_3}(\Sigma)}. \quad (24)$$

where B_1 , B_2 and B_3 refer to the three different bounding boxes shown in the right part of Fig. 2, respectively. As we can see, the calculation process of $KFIoU$ is extremely complex. After analyzing the metrics for bounding box regression of rotated object detection mentioned above, we found that geometric properties of rotated bounding box regression are actually not fully exploited in existing loss functions. Therefore, we propose $FPDIoU$ loss by minimizing the top-left, top-right, bottom-right and bottom-left points distance between predicted bounding box and the groundtruth bounding box for better training deep models of rotated object detection.

3. Proposed Method

It can be proved that four points can define a unique rotated rectangle in 2-D dimension. Inspired by the geometric

properties of rotated rectangle, we designed a novel IoU -based metric named $FPDIoU$ to minimize the top-left, top-right, bottom-right and bottom-left points distance between the predicted bounding box and the groundtruth bounding box directly. In this way, we can improve the accuracy and efficiency of bounding box regression for rotated object detection.

3.1. FPDIoU based on four points distance

After analyzing the advantages and disadvantages of the IoU -based loss functions mentioned above, we start to think how to improve the accuracy and efficiency of bounding box regression. Generally speaking, we use the coordinates of top-left, top-right, bottom-right and bottom-left points to define a unique rotated rectangle. Inspired by the geometric properties of bounding boxes, we designed a novel IoU -based metric named $FPDIoU$ to minimize the top-left, top-right, bottom-right and bottom-left points distance between the predicted bounding box and the groundtruth bounding box directly. The calculation of $FPDIoU$ is summarized in Alg. 1.

In order to ensure the one-to-one correspondence between the coordinates of the predicted bounding box and the groundtruth box no matter how the angle of rotation changes, we sort the coordinates of each bounding box in ascending order of x value. Based on this operation, we can ensure $x_1^A < x_2^A \leq x_3^A < x_4^A$ and $x_1^B < x_2^B \leq x_3^B < x_4^B$. The calculation factors of $FPDIoU$ are shown in Figure 3.

In summary, our proposed $FPDIoU$ simplifies the similarity comparison between two bounding boxes, which can adapt to overlapping or nonoverlapping bounding box regression. Therefore, $FPDIoU$ can be a proper substitute for IoU in all performance measures used in 2D computer vision tasks. In this paper, we only focus on 2D rotated object detection where we can easily derive an analytical solution for $FPDIoU$ to apply it as both metric and loss. The extension to non-axis aligned 3D cases is left as future work.

Algorithm 1 Intersection over Union with Four Points Distance

Require: Two arbitrary convex shapes: $A, B \subseteq \mathbb{S} \in \mathbb{R}^n$, width and height of input image: w, h

Ensure: $FPDIoU(A, B)$

- 1: For A and B , $(x_1^A, y_1^A), (x_2^A, y_2^A), (x_3^A, y_3^A), (x_4^A, y_4^A)$ denote the top-left, top-right, bottom-right and bottom-left point coordinates of A , respectively. $(x_1^B, y_1^B), (x_2^B, y_2^B), (x_3^B, y_3^B), (x_4^B, y_4^B)$ denote the top-left, top-right, bottom-right and bottom-left point coordinates of B , respectively.
- 2: $A.sort(), B.sort()$
- 3: $d_1^2 = (x_1^B - x_1^A)^2 + (y_1^B - y_1^A)^2$
- 4: $d_2^2 = (x_2^B - x_2^A)^2 + (y_2^B - y_2^A)^2$
- 5: $d_3^2 = (x_3^B - x_3^A)^2 + (y_3^B - y_3^A)^2$
- 6: $d_4^2 = (x_4^B - x_4^A)^2 + (y_4^B - y_4^A)^2$
- 7: $FPDIoU(A, B) = \frac{A \cap B}{A \cup B} - \frac{d_1^2 + d_2^2 + d_3^2 + d_4^2}{4 * (w^2 + h^2)}$

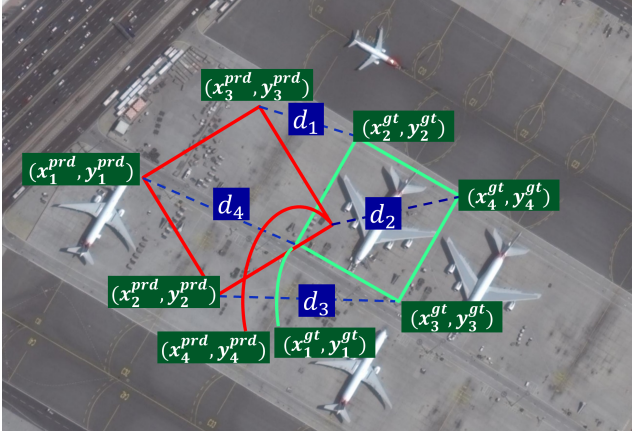


Figure 3: The regression process of our proposed \mathcal{L}_{FPDIoU} . The green box denotes the groundtruth bounding box and the red box denotes the predicted bounding box.

3.2. The proposed FPDIoU loss

In the training phase, each bounding box $\mathcal{B}_{prd} = [x^{prd}, y^{prd}, w^{prd}, h^{prd}, \theta^{prd}]^T$ predicted by the model is forced to approach its groundtruth box $\mathcal{B}_{gt} = [x^{gt}, y^{gt}, w^{gt}, h^{gt}, \theta^{gt}]^T$ by minimizing loss function below:

$$\mathcal{L} = \min_{\Theta} \sum_{\mathcal{B}_{gt} \in \mathbb{B}_{gt}} \mathcal{L}(\mathcal{B}_{gt}, \mathcal{B}_{prd} | \Theta), \quad (25)$$

where \mathbb{B}_{gt} is the set of ground-truth boxes, and Θ is the parameter of deep model for regression. A typical form of \mathcal{L} is ℓ_n -norm, for example, mean-square error (MSE) loss and Smooth- ℓ_1 loss [46], which have been widely adopted in object detection [47]; pedestrian detection [48, 49]; scene text spotting [50, 51]; 3D object detection [52, 53]; pose estimation [54, 55]; and instance segmentation [56, 57]. However, recent researches suggest that ℓ_n -norm-based loss functions are not consistent with the evaluation metric, that

is, interaction over union (IoU), and instead propose IoU -based loss functions [38, 39, 58].

Algorithm 2 IoU and FPDIoU as bounding box losses

Require: The four points' coordinates of the predicted bounding box \mathcal{B}_{prd} and groundtruth bounding box \mathcal{B}_{gt} : $\mathcal{B}_{prd} = (x_1^{prd}, y_1^{prd}, x_2^{prd}, y_2^{prd}, x_3^{prd}, y_3^{prd}, x_4^{prd}, y_4^{prd}), \mathcal{B}_{gt} = (x_1^{gt}, y_1^{gt}, x_2^{gt}, y_2^{gt}, x_3^{gt}, y_3^{gt}, x_4^{gt}, y_4^{gt})$, width and height of input image: w, h .

Ensure: $\mathcal{L}_{RotatedIoU}, \mathcal{L}_{FPDIoU}$

- 1: $d_1^2 = (x_1^{prd} - x_1^{gt})^2 + (y_1^{prd} - y_1^{gt})^2$
- 2: $d_2^2 = (x_2^{prd} - x_2^{gt})^2 + (y_2^{prd} - y_2^{gt})^2$
- 3: $d_3^2 = (x_3^{prd} - x_3^{gt})^2 + (y_3^{prd} - y_3^{gt})^2$
- 4: $d_4^2 = (x_4^{prd} - x_4^{gt})^2 + (y_4^{prd} - y_4^{gt})^2$
- 5: Calculating rotated IoU of \mathcal{B}_{gt} and \mathcal{B}_{prd} as $RotatedIoU(\mathcal{B}_{gt}, \mathcal{B}_{prd})$.
- 6: $FPDIoU = RotatedIoU(\mathcal{B}_{gt}, \mathcal{B}_{prd}) - \frac{d_1^2 + d_2^2 + d_3^2 + d_4^2}{4 * (h^2 + w^2)}$
- 7: $\mathcal{L}_{RotatedIoU} = 1 - RotatedIoU, \mathcal{L}_{FPDIoU} = 1 - FPDIoU$.

Since back-propagating min, max and piece-wise linear functions, e.g. Relu, are feasible, it can be shown that every component in Alg. 2 has a well-behaved derivative. Therefore, $RotatedIoU$, $GIoU$, $DIoU$, $PIoU$, $KFIoU$ and $FPDIoU$ can be directly used as loss functions, i.e. $\mathcal{L}_{RotatedIoU}, \mathcal{L}_{GIoU}, \mathcal{L}_{DIoU}, \mathcal{L}_{PIoU}, \mathcal{L}_{KFIoU}$ and \mathcal{L}_{FPDIoU} , for optimizing object detection or instance segmentation models. In this case, we are directly optimizing a metric as loss, which is an optimal choice for the metric. However, in all non-overlapping cases, $RotatedIoU$ has zero gradient, which affects both training accuracy and convergence speed. $FPDIoU$, in contrast, has a gradient in all possible cases, including non-overlapping situations.

Considering the groundtruth bounding box, \mathcal{B}_{gt} is a rotated rectangle with area bigger than zero, i.e. $A^{gt} > 0$. As a result, union area $\mathcal{U} > 0$ for any predicted bounding box

$\mathcal{B}_{prd} = (x_1^{prd}, y_1^{prd}, x_2^{prd}, y_2^{prd}, x_3^{prd}, y_3^{prd}, x_4^{prd}, y_4^{prd}) \in \mathbb{R}^8$. This ensures that the denominator in IoU cannot be zero for any predicted value of outputs. In addition, for any values of $\mathcal{B}_{prd} = (x_1^{prd}, y_1^{prd}, x_2^{prd}, y_2^{prd}, x_3^{prd}, y_3^{prd}, x_4^{prd}, y_4^{prd}) \in \mathbb{R}^8$, the union area is always bigger than the intersection area, i.e. $\mathcal{U} \geq \mathcal{I}$. As a result, \mathcal{L}_{FPDIoU} is always bounded, i.e. $0 \leq \mathcal{L}_{FPDIoU} < 2, \forall \mathcal{B}_{prd} \in \mathbb{R}^8$.

We use the one-stage detector RTMDET and weakly-supervised detector H2RBox as the baseline. The rotated rectangle can be represented by (x, y, w, h, θ) or $((x_1, y_1), (x_2, y_2), (x_3, y_3), (x_4, y_4))$. The two expressions mentioned above can be converted into each other without affecting the regression results. The relationship between them can be formulated as follows:

$$x = \frac{x_2 + x_1}{2}, y = \frac{y_2 + y_1}{2} \quad (26)$$

$$w = \sqrt{(x_2 - x_1)^2 + (y_2 - y_1)^2}, h = \sqrt{(x_3 - x_1)^2 + (y_3 - y_1)^2} \quad (27)$$

$$\theta = \arctan \frac{y_2 - y_3}{x_2 - x_3} \quad (28)$$

where x, y, w, h denote the rotated bounding box's center coordinates, width and height, respectively. θ denotes the rotation angle of rotated bounding box. $(x_1, y_1), (x_2, y_2), (x_3, y_3), (x_4, y_4)$ represent the top-left, top-right, bottom-right and bottom-left points coordinates, respectively. As Eq.26-28 shows, all of the key factors of rotated bounding box can be represented by four points coordinates, which means our proposed *FPDIoU* is not only considerate, but also simplifies the calculation process of rotated bounding box regression.

4. Experiments

4.1. Datasets

We choose some of the popular rotated object detection datasets to evaluate the performance of our proposed loss function. The details are shown as follow.

DOTA [17] is one of the largest datasets for oriented object detection in aerial images with three released versions: DOTA-v1.0, DOTA-v1.5 and DOTA-v2.0. DOTA-v1.0 contains 15 common categories, 2,806 images and 188,282 instances. The images of DOTA-v1.5 are the same as DOTA-v1.0, but some of the small instances (less than 10 pixels) are also annotated. Moreover, a new category, containing 402,089 instances in total is added in this version. While DOTA-v2.0 contains 18 common categories, 11,268 images and 1,793,658 instances. We divide the images into 600*600 subimages with an overlap of 150 pixels and scale it to 800*800.

HRSC2016 [19] is a publicly available remote sensing image ship dataset contains images from two scenarios with ships on sea and close inshore. The training, validation and test set include 436, 181 and 444 images, covering 28 object classes.

DIOR [18] is a large-scale benchmark dataset for rotated object detection of optical remote sensing images. The dataset contains 23,463 images and 192,472 instances, covering 20 object classes. The 20 object classes are airplanes, airports, baseball fields, basketball courts, bridges, chimneys, dams, highway service areas, highway toll booths, ports, golf courses, surface athletic fields, flyovers, ships, stadiums, storage tanks, tennis courts, train stations, vehicles and wind mills.

ICDAR 2017 RRC-MLT [20] is a multilingual and multi-directional scene text detection and recognition dataset, which includes 9 languages including Chinese, Japanese, Korean, English, French, Arabic, Italian, German, and India. The scale of training, validation, and testing sets are 7200,

1800 and 9000, respectively.

ICDAR 2019 RRC-MLT [21] is a multilingual and multi-directional scene text detection and recognition dataset, including 10 languages such as Arabic, English, Japanese, Korean, and Chinese. The scale of training and testing sets are all 10 000.

4.2. Experimental Settings

The experimental environment of rotated object detectors described in this paper is as follows: the memory is 32GB, the operating system is windows 11, the CPU is Intel i9-12900k, and the graphics card is NVIDIA Geforce RTX 3090 with 24GB memory. In order to conduct a fair comparison, all of the experiments are implemented with PyTorch [59].

4.3. Evaluation Protocol

In this paper, we used mean Average Precision (mAP) over different class labels for a specific value of *IoU* threshold in order to determine true positives and false positives. The main performance measure of rotated object detection used in our experiments is shown by precision and mAP@0.5:0.95. We report the mAP value for *IoU* thresholds equal to 0.5 and 0.75, shown as AP50 and AP75 in the tables. As for arbitrary orientation scene text spotting, the main performance measurements used in our experiments are shown by Precision, Recall and Hmean.

4.4. Experimental Results

4.4.1. Comparison with the existing losses

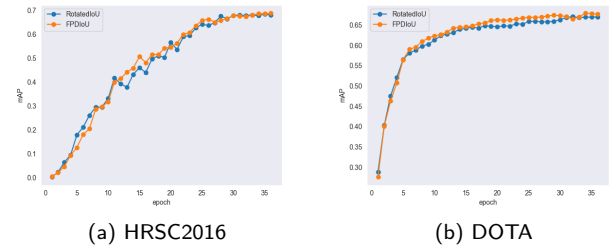


Figure 4: Comparison of mAP value trends on HRSC2016 and DOTA test set training with RTMDet [34].

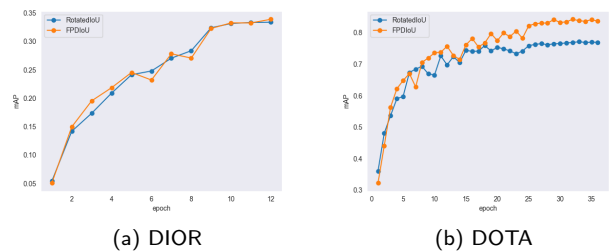


Figure 5: Comparison of mAP value trends on DIOR and DOTA test set training with H2RBox [35].

Table 1

Comparison between the performance of H2RBox [35] trained using its own loss ($\mathcal{L}_{RotatedIoU}$) as well as \mathcal{L}_{GIoU} , \mathcal{L}_{DIoU} , \mathcal{L}_{PIoU} , \mathcal{L}_{KFIoU} and \mathcal{L}_{FPDIoU} . The results are reported on the test set of DOTA-v1.0.

Loss \ Evaluation	mAP	AP50	AP75	speed(iter/s)
$\mathcal{L}_{RotatedIoU}$	30.84	63	25.83	1.11
\mathcal{L}_{GIoU}	31.94	64	26.93	1.05
Relative improv(%)	3.56	1.58	4.25	-5.4
\mathcal{L}_{DIoU}	32.08	65.8	27.63	0.99
Relative improv(%)	4.02	4.4	6.96	-10.8
\mathcal{L}_{PIoU}	33.28	66.6	28.23	0.91
Relative improv(%)	7.91	5.71	9.29	-18.01
\mathcal{L}_{KFIoU}	35.18	67.2	27.63	0.89
Relative improv(%)	14.07	4.4	6.96	-10.8
\mathcal{L}_{FPDIoU}	40.13	71.74	38.41	0.73
Relative improv(%)	30.12	13.87	48.7	-34.2

Table 2

Comparison between the performance of H2RBox [35] trained using its own loss ($\mathcal{L}_{RotatedIoU}$) as well as \mathcal{L}_{GIoU} , \mathcal{L}_{DIoU} , \mathcal{L}_{PIoU} , \mathcal{L}_{KFIoU} and \mathcal{L}_{FPDIoU} . The results are reported on the test set of DIOR.

Loss \ Evaluation	mAP	AP50	AP75	speed(iter/s)
$\mathcal{L}_{RotatedIoU}$	33.39	56.4	33.4	3.9
\mathcal{L}_{GIoU}	33.56	56.7	33.45	3.75
Relative improv(%)	0.51	0.53	0.14	-5.4
\mathcal{L}_{DIoU}	33.69	57.1	33.49	3.85
Relative improv(%)	0.89	1.24	0.26	-1.28
\mathcal{L}_{PIoU}	33.78	57.3	33.49	3.88
Relative improv(%)	1.16	1.59	0.26	-0.51
\mathcal{L}_{KFIoU}	33.8	57.6	33.5	4.01
Relative improv(%)	1.22	2.12	0.29	2.82
\mathcal{L}_{FPDIoU}	33.9	57.7	33.5	4.17
Relative improv(%)	1.52	2.3	0.29	6.9

We used the original CSPDarkNet implementation of RTMDET released by [34] and the official implementation of H2RBox to conduct our experiments. To train RTMDET and H2RBox using *RotatedIoU*, *GIoU*, *DIoU*, *PIoU*, *KFIoU* and *FPDIoU* losses, we simply replace the bounding box regression *RotatedIoU* loss with \mathcal{L}_{FPDIoU} loss explained in Alg. 2.

Results of object detection for natural scenes

In order to compare the regression process between $\mathcal{L}_{RotatedIoU}$ and \mathcal{L}_{FPDIoU} , we recorded the mAP values during the training process using $\mathcal{L}_{RotatedIoU}$ and \mathcal{L}_{FPDIoU} . As Figure 4 and Figure 5 shows, the model training with our proposed \mathcal{L}_{FPDIoU} reached the best performance earlier than training with $\mathcal{L}_{RotatedIoU}$, which means our proposed \mathcal{L}_{FPDIoU} has faster convergence speed and higher accuracy on rotated object detection tasks.

To make more intuitive comparison of the performance between the existing *IOU*-based loss functions and \mathcal{L}_{FPDIoU}

Table 3

Comparison between the performance of RTMDET [34] trained using its own loss ($\mathcal{L}_{RotatedIoU}$) as well as \mathcal{L}_{GIoU} , \mathcal{L}_{DIoU} , \mathcal{L}_{PIoU} , \mathcal{L}_{KFIoU} and \mathcal{L}_{FPDIoU} . The results are reported on the test set of DOTA-v1.0.

Loss \ Evaluation	mAP	AP50	AP75	speed(iter/s)
$\mathcal{L}_{RotatedIoU}$	46.16	74.94	49.06	2.73
\mathcal{L}_{GIoU}	46.33	75.03	49.2	2.33
Relative improv(%)	0.36	0.12	0.28	-14.65
\mathcal{L}_{DIoU}	46.73	75.2	49.55	2.05
Relative improv(%)	1.23	0.34	0.99	-24.9
\mathcal{L}_{PIoU}	47.1	75.28	48.23	0.91
Relative improv(%)	7.91	5.71	9.29	-18.01
\mathcal{L}_{KFIoU}	47.28	75.38	49.63	0.89
Relative improv(%)	2.42	0.58	1.16	-10.8
\mathcal{L}_{FPDIoU}	47.37	75.38	50.71	3.75
Relative improv(%)	2.62	0.58	3.36	37.36

Table 4

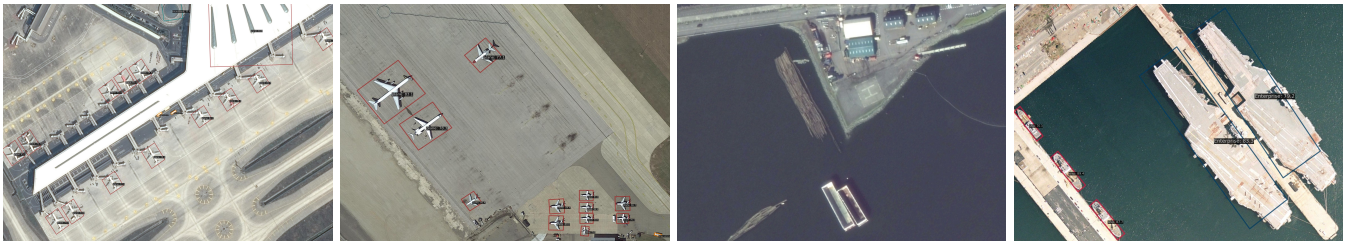
Comparison between the performance of RTMDET [34] trained using its own loss ($\mathcal{L}_{RotatedIoU}$) as well as \mathcal{L}_{GIoU} , \mathcal{L}_{DIoU} , \mathcal{L}_{PIoU} , \mathcal{L}_{KFIoU} and \mathcal{L}_{FPDIoU} . The results are reported on the test set of HRSC2016.

Loss \ Evaluation	mAP	AP50	AP75	speed(iter/s)
$\mathcal{L}_{RotatedIoU}$	65.69	70.3	61.1	54.94
\mathcal{L}_{GIoU}	65.77	70.33	61.2	62.3
Relative improv(%)	0.12	0.04	0.16	13.39
\mathcal{L}_{DIoU}	65.97	70.35	61.6	66.2
Relative improv(%)	0.42	0.07	0.81	20.49
\mathcal{L}_{PIoU}	66.1	70.35	61.85	69.5
Relative improv(%)	0.62	0.07	1.22	26.5
\mathcal{L}_{KFIoU}	66.25	70.38	62.1	73.3
Relative improv(%)	0.85	0.11	1.63	33.41
\mathcal{L}_{FPDIoU}	66.37	70.4	62.3	81.96
Relative improv(%)	1.03	0.14	1.96	49.18

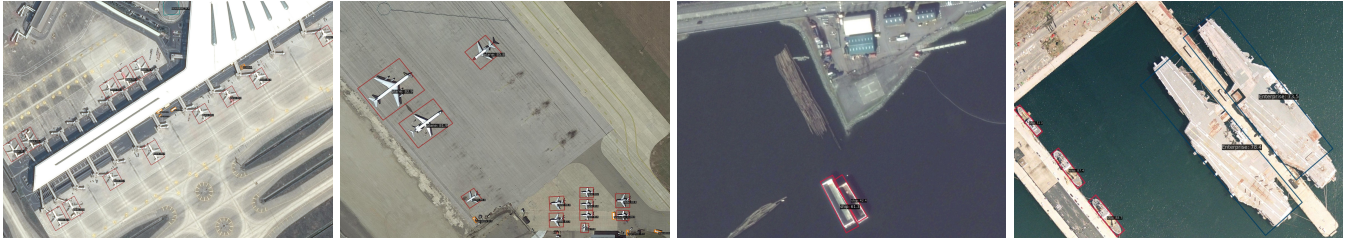
proposed by us, we conduct further experiments using $\mathcal{L}_{RotatedIoU}$, \mathcal{L}_{GIoU} , \mathcal{L}_{DIoU} , \mathcal{L}_{PIoU} , \mathcal{L}_{KFIoU} and \mathcal{L}_{FPDIoU} to train the SOTA rotated object detectors RTMDET[34] and H2RBox[35]. We give the comparison results from two aspects including accuracy and efficiency. The experimental results are shown as Table 1-4.

As we can see, no matter which rotated object detectors we use, the models training with our proposed \mathcal{L}_{FPDIoU} achieve better performance than using existing losses for rotated object detection. In most of the cases, the *mAP* values and inference speed increased obviously using \mathcal{L}_{FPDIoU} .

As Figure 6 and 7 shows, the rotated object detectors training with our proposed \mathcal{L}_{FPDIoU} achieve better performance than training with their original loss functions. Especially, our visualize results have less redundancy and higher integrity. For example, the terminal was misrecognized as plane in first image of Figure 6(a) and the roundabout is not

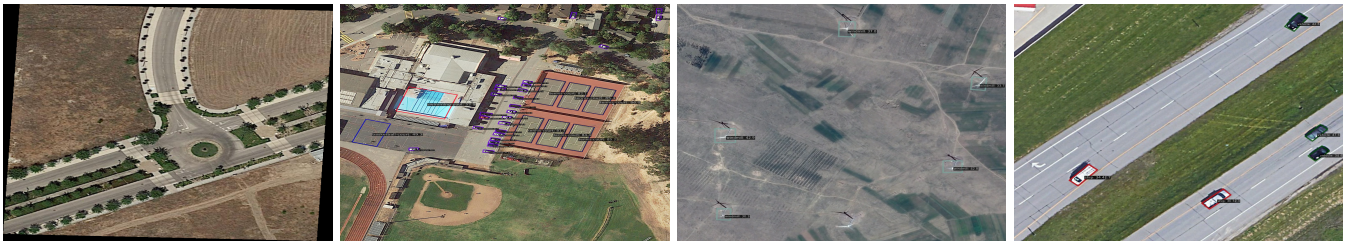


(a) Rotated object detection results training with $\mathcal{L}_{RotatedIoU}$

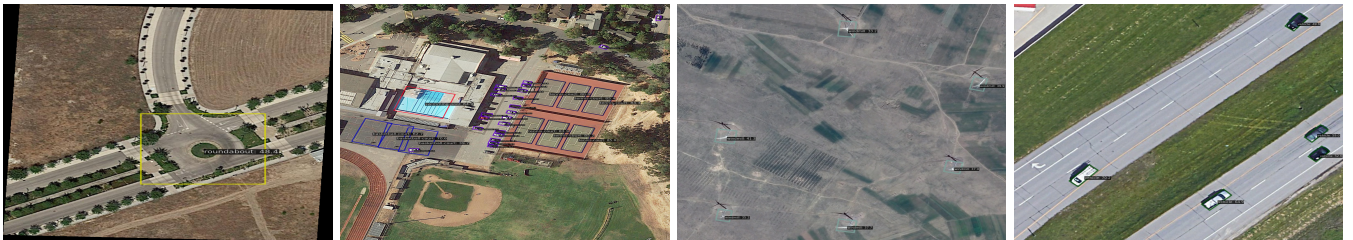


(b) Rotated object detection results training with \mathcal{L}_{FPDIoU}

Figure 6: Rotated object detection results from the test set of DOTA [17] and HRSC2016 [19] using RTMDet [34] trained using $\mathcal{L}_{RotatedIoU}$ and \mathcal{L}_{FPDIoU} losses.



(a) Rotated object detection results training with $\mathcal{L}_{RotatedIoU}$



(b) Rotated object detection results training with \mathcal{L}_{FPDIoU}

Figure 7: Rotated object detection results from the test set of DOTA [17] and DIOR [18] using H2RBox [35] trained using $\mathcal{L}_{RotatedIoU}$ and \mathcal{L}_{FPDIoU} losses.

detected in first image of Figure 7(a), some trucks were not detected in the second image of Figure 6(a).

In order to better reveal the performance of different loss functions for bounding box regression of rotated object detection, we provide some of the visualization results as Figure 6 shows. As we can see, the rotated object detection results provided by model training with our proposed \mathcal{L}_{FPDIoU} are with less redundancy and higher accuracy than model training with $\mathcal{L}_{RotatedIoU}$.

Results of arbitrary orientation scene text spotting

In order to further verify the effectiveness of the bounding box regression loss function described in this chapter in the arbitrary orientation scene text spotting task, we selected

the ICDAR 2017 RRC-MLT and ICDAR 2019 RRC-MLT datasets to be used on the RTMDet [34] model. The experimental results are shown as Table 5 and Table 6. It can be seen that the performance and efficiency of \mathcal{L}_{FPDIoU} in any direction text detection task proposed in this chapter are still significantly improved, and the accuracy is especially improved, indicating that the \mathcal{L}_{FPDIoU} proposed by ourselves can output more accurate and less redundant text detection results in any direction. As Figure 8 shows, the arbitrary orientation scene text spotter training with our proposed \mathcal{L}_{FPDIoU} achieve better performance than training with its original loss functions. Especially, our visualize results have less redundancy and higher integrity. For example, The text in



Figure 8: Arbitrary orientation scene text spotting results from the test set of ICDAR 2017 RRC-MLT [20] and ICDAR 2019 RRC-MLT [21] using RTMDET [34] trained using $\mathcal{L}_{RotatedIoU}$ and \mathcal{L}_{FPDIoU} losses.

Table 5

Comparison between the performance of RTMDET [34] trained using its own loss ($\mathcal{L}_{RotatedIoU}$) as well as \mathcal{L}_{GIoU} , \mathcal{L}_{DIOU} , \mathcal{L}_{PIoU} , \mathcal{L}_{KFIoU} and \mathcal{L}_{FPDIoU} . The results are reported on the test set of ICDAR 2017 RRC-MLT.

Loss \ Evaluation	P	R	H	speed(iter/s)
$\mathcal{L}_{RotatedIoU}$	82.55	54.77	65.85	2.29
\mathcal{L}_{GIoU}	82.94	54.87	65.93	2.32
Relative improv(%)	0.47	0.18	0.12	1.31
\mathcal{L}_{DIOU}	83.08	54.1	65.98	2.39
Relative improv(%)	0.64	-1.2	0.19	4.36
\mathcal{L}_{PIoU}	83.28	54.26	66.03	2.43
Relative improv(%)	0.88	-0.93	0.27	6.11
\mathcal{L}_{KFIoU}	83.98	54.29	65.96	2.89
Relative improv(%)	1.73	-0.87	0.16	26.2
\mathcal{L}_{FPDIoU}	84.19	54.33	66.04	2.93
Relative improv(%)	1.98	-0.8	0.28	27.94

the first red banner in the middle of the first image of Figure 8(a) is not detected and the vertical text is not detected in third image of Figure 8(a).

4.4.2. Comparison with the State-of-the-art methods

In order to verify the performance of our proposed $FPDIoU$, we conduct experiments to compare with the state-of-the-art rotated object detection methods. The experimental results are shown as Table 7, which compares recent detectors on DOTA-v1.0, as categorized by single-, refine-, and two-stage based methods. Due to different image resolution, network structure, training strategies and various tricks between different methods, we cannot make absolutely fair comparisons. In terms of overall performance, our method has achieved the best performance so far, at around 81.33%.

Table 6

Comparison between the performance of RTMDET [34] trained using its own loss ($\mathcal{L}_{RotatedIoU}$) as well as \mathcal{L}_{GIoU} , \mathcal{L}_{DIOU} , \mathcal{L}_{PIoU} , \mathcal{L}_{KFIoU} and \mathcal{L}_{FPDIoU} . The results are reported on the test set of ICDAR 2019 RRC-MLT.

Loss \ Evaluation	P	R	H	speed(iter/s)
$\mathcal{L}_{RotatedIoU}$	83.20	55.63	66.68	2.29
\mathcal{L}_{GIoU}	83.39	55.2	66.72	2.22
Relative improv(%)	3.56	1.58	4.25	-5.4
\mathcal{L}_{DIOU}	83.60	55.33	66.75	2.39
Relative improv(%)	0.48	0.53	0.10	4.36
\mathcal{L}_{PIoU}	83.68	55.6	66.83	2.41
Relative improv(%)	0.57	0.05	0.22	5.24
\mathcal{L}_{KFIoU}	84.18	55.72	66.86	2.41
Relative improv(%)	1.17	0.16	0.26	5.24
\mathcal{L}_{FPDIoU}	84.84	55.21	66.89	2.43
Relative improv(%)	1.97	0.75	0.31	6.11

5. Conclusion

In this paper, we introduced a new metric named $FPDIoU$ based on minimum points distance for comparing any two arbitrary bounding boxes. We proved that this new metric has all of the appealing properties which existing IoU -based metrics have while simplifying its calculation. It will be a better choice in all performance measures in 2D/3D vision tasks relying on the IoU metric.

We also proposed a loss function called \mathcal{L}_{FPDIoU} for bounding box regression. By incorporating it into the state-of-the-art rotated object detection algorithms, we consistently improved their performance on popular rotated object detection benchmarks such as DOTA, DIOR and HRSC2016

Table 7

Rotated object detection results test on DOTA-v1.0 test dataset. Red and blue: top two performances

	Method	PL	BD	BR	GTF	SV	LV	SH	TC	BC	ST	SBF	RA	HA	SP	HC	mAP_{50}
Single-stage	PloU[42]	80.90	69.70	24.10	60.20	38.30	64.40	64.80	90.90	77.20	70.40	46.50	37.10	57.10	61.90	64.00	60.50
	O^2 -DNet[60]	89.31	82.14	47.33	61.21	71.32	74.03	78.62	90.76	82.23	81.36	60.93	60.17	58.21	66.98	61.03	71.04
	DAL[25]	88.61	79.69	46.27	70.37	65.89	76.10	78.53	90.84	79.98	78.41	58.71	62.02	69.23	71.32	60.65	71.78
	P-RSDet[61]	88.58	77.83	50.44	69.29	71.10	75.79	78.66	90.88	80.10	81.71	57.92	63.03	66.30	69.77	63.13	72.30
	BBAVectors[62]	88.35	79.96	50.69	62.18	78.43	78.98	87.94	90.85	83.58	84.35	54.13	60.24	65.22	64.28	55.70	72.32
	DRN[24]	89.71	82.34	47.22	64.10	76.22	74.43	85.84	90.57	86.18	84.89	57.65	61.93	69.30	69.63	58.48	73.23
	DCL[63]	89.10	84.13	50.15	73.57	71.48	58.13	78.00	90.89	86.64	86.78	67.97	67.25	65.63	74.06	67.05	74.06
	PolarDet[64]	89.65	87.07	48.14	70.97	78.53	80.34	87.45	90.76	85.63	86.87	61.64	70.32	71.92	73.09	67.15	76.64
	GWD[43]	86.96	83.88	54.36	77.53	74.41	68.48	80.34	86.62	83.41	85.55	73.47	67.77	72.57	75.76	73.40	76.30
	KFIoU[45]	89.46	85.72	54.94	80.37	77.16	69.23	80.90	90.79	87.79	86.13	73.32	68.11	75.23	71.61	69.49	77.35
Refine-stage	CFC-Net[65]	89.08	80.41	52.41	70.02	76.28	78.11	87.21	90.89	84.47	85.64	60.51	61.52	67.82	68.02	50.09	73.50
	R3Det[26]	89.80	83.77	48.11	66.77	78.76	83.27	87.84	90.82	85.38	85.51	65.67	62.68	67.53	78.56	72.62	76.47
	CFA[66]	89.08	83.20	54.37	66.87	81.23	80.96	87.17	90.21	84.32	86.09	52.34	69.94	75.52	80.76	67.96	76.67
	DAL[25]	89.69	83.11	55.03	71.00	78.30	81.90	88.46	90.89	84.97	87.46	64.41	65.65	76.86	72.09	64.35	76.95
	DCL[63]	89.26	83.60	53.54	72.76	79.04	82.56	87.31	90.67	86.59	86.98	67.49	66.88	73.29	70.56	69.99	77.37
	RIDet[67]	89.31	80.77	54.07	76.38	79.81	81.99	89.13	90.72	83.58	87.22	64.42	67.56	78.08	79.17	62.07	77.62
	S2A-Net[27]	88.89	83.60	57.74	81.95	79.94	83.19	89.11	90.78	84.87	87.81	70.30	68.25	78.30	77.01	69.58	79.42
	R3Det-GWD[43]	89.66	84.99	59.26	82.19	78.97	84.83	87.70	90.21	86.54	86.85	73.47	67.77	76.92	79.22	74.92	80.23
	R3Det-KLD[44]	89.92	85.13	59.19	81.33	78.82	84.38	87.50	89.80	87.33	87.00	72.57	71.35	77.12	79.34	78.68	80.63
	R3Det-KFIoU[45]	88.89	85.14	60.05	81.13	81.78	85.71	88.27	90.87	87.12	87.91	69.77	73.70	79.25	81.31	74.56	81.03
Two-stage	ICN[28]	81.40	74.30	47.70	70.30	64.90	67.80	70.00	90.80	79.10	78.20	53.60	62.90	67.00	64.20	50.20	68.20
	RoI-Trans[29]	88.64	78.52	43.44	75.92	68.81	73.68	83.59	90.74	77.27	81.46	58.39	53.54	62.83	58.93	47.67	69.56
	SCRDet[30]	89.98	80.65	52.09	68.36	68.36	60.32	72.41	90.85	87.94	86.86	65.02	66.68	66.25	68.24	65.21	72.61
	Gliding Vertex[32]	89.64	85.00	52.26	77.34	73.01	73.14	86.82	90.74	79.02	86.81	59.55	70.91	72.94	70.86	57.32	75.02
	Mask OBB[31]	89.56	85.95	54.21	72.90	76.52	74.16	85.63	89.85	83.81	86.48	54.89	69.64	73.94	69.06	63.32	75.33
	CenterMap[68]	89.83	84.41	54.60	70.25	77.66	78.32	87.19	90.66	84.89	85.27	56.46	69.23	74.13	71.56	66.06	76.03
	CSL[69]	90.25	85.53	54.64	75.31	70.44	73.51	77.62	90.84	86.15	86.69	69.60	68.04	73.83	71.10	68.93	76.17
	RSDet-II[70]	89.93	84.45	53.77	74.35	71.52	78.31	78.12	91.14	87.35	86.93	65.64	65.17	75.35	79.74	63.31	76.34
	SCRDet++[71]	90.05	84.39	55.44	73.99	77.54	71.11	86.05	90.67	87.32	87.08	69.62	68.90	73.74	71.29	65.08	76.81
	ReDet[33]	88.81	82.48	60.83	80.82	78.34	86.06	88.31	90.87	88.77	87.03	68.65	66.90	79.26	79.71	74.67	80.10
	Oriented R-CNN[72]	89.84	85.43	61.09	79.82	79.71	85.35	88.82	90.88	86.68	87.73	72.21	70.80	82.42	78.18	74.11	80.87
	RoI-Trans-KFIoU[45]	89.44	84.41	62.22	82.51	80.10	86.07	88.68	90.90	87.32	88.38	72.80	71.95	78.96	74.95	75.27	80.93
	RTMDET-FPDIoU(Ours)	89.34	84.41	60.22	78.18	81.50	85.30	88.84	90.87	86.41	87.55	72.70	71.95	78.96	80.31	75.27	81.33

using the commonly used performance measures based average precision. Since the optimal loss for a metric is the metric itself, our $FPDIoU$ loss can be used as the optimal bounding box regression loss in all applications which require 2D bounding box regression.

As for future work, we would like to conduct further experiments on some downstream tasks based on rotated object detection, including arbitrary orientation scene text spotting, person re-identification and so on. With the above experiments, we can further verify the generalization ability of our proposed loss functions.

Declaration of competing interest

The authors declare that they have no known competing financial interests or personal relationships that could have appeared to influence the work reported in this paper.

CRedit authorship contribution statement

Siliang Ma: Conceptualization, Methodology, Programming, Data creation, Writing - original draft. **Yong Xu:** Supervision, Writing-Reviewing and Editing.

Acknowledgements

This work was supported by the National Natural Science Foundation of China(No.62072188).

References

- [1] J. Redmon and A. Farhadi. Yolo9000: Better, faster, stronger. In *IEEE Conference on Computer Vision & Pattern Recognition*, pages 6517–6525, 2017.
- [2] Ali Farhadi Joseph Redmon. Yolov3: An incremental improvement. *ArXiv*, abs/1804.02767, 2018.
- [3] A. Bochkovskiy, C. Y. Wang, and Hym Liao. Yolov4: Optimal speed and accuracy of object detection. 2020.
- [4] C. Y. Wang, A. Bochkovskiy, and Hym Liao. Yolov7: Trainable bag-of-freebies sets new state-of-the-art for real-time object detectors. 2022.
- [5] Qiang Chen, Yingming Wang, Tong Yang, Xiangyu Zhang, Jian Cheng, and Jian Sun. You only look one-level feature. In *2021 IEEE/CVF Conference on Computer Vision and Pattern Recognition (CVPR)*, pages 13034–13043, 2021.
- [6] Wided Souidene Mseddi, Rafik Ghali, Marwa Jmal, and Rabah Attia. Fire detection and segmentation using yolov5 and u-net. In *2021 29th European Signal Processing Conference (EUSIPCO)*, pages 741–745, 2021.
- [7] S. Ren, K. He, R. Girshick, and J. Sun. Faster r-cnn: Towards real-time object detection with region proposal networks. In *NIPS*, 2016.
- [8] Ze Yang, Shaohui Liu, Han Hu, Liwei Wang, and Stephen Lin. Repoints: Point set representation for object detection. In *Proceedings of*

- the *IEEE/CVF International Conference on Computer Vision*, pages 9657–9666, 2019.
- [9] Tsung-Yi Lin, Priya Goyal, Ross Girshick, Kaiming He, and Piotr Dollár. Focal loss for dense object detection. In *Proceedings of the IEEE international conference on computer vision*, pages 2980–2988, 2017.
 - [10] Jiahui Yu, Yuning Jiang, Zhangyang Wang, Zhimin Cao, and Thomas Huang. Unitbox: An advanced object detection network. In *Proceedings of the 24th ACM International Conference on Multimedia*, MM '16, page 516–520, New York, NY, USA, 2016. Association for Computing Machinery.
 - [11] Marius Cordts, Mohamed Omran, Sebastian Ramos, Timo Rehfeld, Markus Enzweiler, Rodrigo Benenson, Uwe Franke, Stefan Roth, and Bernt Schiele. The cityscapes dataset for semantic urban scene understanding. 06 2016.
 - [12] M. R. Everingham, Sma Eslami, L. J. Gool, Cki Williams, J. M. Winn, and A. Zisserman. The pascal visual object classes challenge. *International Journal of Computer Vision*, 2015.
 - [13] Hassan Alhajja, Siva Mustikovela, Lars Mescheder, Andreas Geiger, and Carsten Rother. Augmented reality meets computer vision : Efficient data generation for urban driving scenes. *International Journal of Computer Vision*, 126, 09 2018.
 - [14] Bolei Zhou, Hang Zhao, Xavier Puig, Sanja Fidler, Adela Barriuso, and Antonio Torralba. Scene parsing through ade20k dataset. In *Proceedings of the IEEE conference on computer vision and pattern recognition*, pages 633–641, 2017.
 - [15] Tsung Yi Lin, Michael Maire, Serge Belongie, James Hays, and C. Lawrence Zitnick. Microsoft coco: Common objects in context. *Springer International Publishing*, 2014.
 - [16] Laura Leal-Taixé, Anton Milan, Ian Reid, Stefan Roth, and Konrad Schindler. Motchallenge 2015: Towards a benchmark for multi-target tracking. *arXiv preprint arXiv:1504.01942*, 2015.
 - [17] Gui-Song Xia, Xiang Bai, Jian Ding, Zhen Zhu, Serge Belongie, Jiebo Luo, Mihai Datcu, Marcello Pelillo, and Liangpei Zhang. Dota: A large-scale dataset for object detection in aerial images. In *2018 IEEE/CVF Conference on Computer Vision and Pattern Recognition*, pages 3974–3983, 2018.
 - [18] Ke Li, Gang Wan, Gong Cheng, Liqiu Meng, and Junwei Han. Object detection in optical remote sensing images: A survey and a new benchmark. *ISPRS Journal of Photogrammetry and Remote Sensing*, 159:296–307, 2020.
 - [19] Zikun Liu., Liu Yuan., Lubin Weng., and Yiping Yang. A high resolution optical satellite image dataset for ship recognition and some new baselines. In *Proceedings of the 6th International Conference on Pattern Recognition Applications and Methods - ICPRAM*, pages 324–331. INSTICC, SciTePress, 2017.
 - [20] Nibal Nayef, Fei Yin, Imen Bizid, Hyunsoo Choi, Yuan Feng, Dimosthenis Karatzas, Zhenbo Luo, Umapada Pal, Christophe Rigaud, Joseph Chazalon, et al. Icdar2017 robust reading challenge on multi-lingual scene text detection and script identification-rrc-mlt. In *2017 14th IAPR international conference on document analysis and recognition (ICDAR)*, volume 1, pages 1454–1459. IEEE, 2017.
 - [21] Nibal Nayef, Yash Patel, Michal Busta, Pinaki Nath Chowdhury, Dimosthenis Karatzas, Wafa Khelif, Jiri Matas, Umapada Pal, Jean-Christophe Burie, Cheng-lin Liu, et al. Icdar2019 robust reading challenge on multi-lingual scene text detection and recognition—rrc-mlt-2019. In *2019 International conference on document analysis and recognition (ICDAR)*, pages 1582–1587. IEEE, 2019.
 - [22] Ross Girshick. Fast r-cnn. In *Proceedings of the 2015 IEEE International Conference on Computer Vision (ICCV)*, ICCV'15, pages 1440–1448, USA, 2015. IEEE Computer Society.
 - [23] T. Y. Lin, P. Dollár, R. Girshick, K. He, B. Hariharan, and S. Belongie. Feature pyramid networks for object detection. *IEEE Computer Society*, 2017.
 - [24] Xingjia Pan, Yuqiang Ren, Kekai Sheng, Weiming Dong, Haolei Yuan, Xiaowei Guo, Chongyang Ma, and Changsheng Xu. Dynamic refinement network for oriented and densely packed object detection. In *2020 IEEE/CVF Conference on Computer Vision and Pattern Recognition (CVPR)*, pages 11204–11213, 2020.
 - [25] Qi Ming, Zhiqiang Zhou, Lingjuan Miao, Hongwei Zhang, and Linhao Li. Dynamic anchor learning for arbitrary-oriented object detection. In *Proceedings of the AAAI Conference on Artificial Intelligence*, volume 35, pages 2355–2363, 2021.
 - [26] Xue Yang, Junchi Yan, Ziming Feng, and Tao He. R3det: Refined single-stage detector with feature refinement for rotating object. In *Proceedings of the AAAI Conference on Artificial Intelligence*, volume 35, pages 3163–3171, 2021.
 - [27] Jiaming Han, Jian Ding, Jie Li, and Gui-Song Xia. Align deep features for oriented object detection. *IEEE Transactions on Geoscience and Remote Sensing*, 60:1–11, 2022.
 - [28] Seyed Majid Azimi, Eleonora Vig, Reza Bahmanyar, Marco Körner, and Peter Reinartz. Towards multi-class object detection in unconstrained remote sensing imagery. In C. V. Jawahar, Hongdong Li, Greg Mori, and Konrad Schindler, editors, *Computer Vision – ACCV 2018*, pages 150–165, Cham, 2019. Springer International Publishing.
 - [29] Jian Ding, Nan Xue, Yang Long, Gui-Song Xia, and Qikai Lu. Learning roi transformer for oriented object detection in aerial images. In *2019 IEEE/CVF Conference on Computer Vision and Pattern Recognition (CVPR)*, pages 2844–2853, 2019.
 - [30] Xue Yang, Jirui Yang, Junchi Yan, Yue Zhang, Tengfei Zhang, Zhi Guo, Xian Sun, and Kun Fu. Scrdet: Towards more robust detection for small, cluttered and rotated objects. In *2019 IEEE/CVF International Conference on Computer Vision (ICCV)*, pages 8231–8240, 2019.
 - [31] Jinwang Wang, Jian Ding, Haowen Guo, Wensheng Cheng, Ting Pan, and Wen Yang. Mask obb: A semantic attention-based mask oriented bounding box representation for multi-category object detection in aerial images. *Remote. Sens.*, 11:2930, 2019.
 - [32] Yongchao Xu, Mingtao Fu, Qimeng Wang, Yukang Wang, Kai Chen, Gui-Song Xia, and Xiang Bai. Gliding vertex on the horizontal bounding box for multi-oriented object detection. *IEEE Transactions on Pattern Analysis and Machine Intelligence*, 43(4):1452–1459, 2021.
 - [33] Jiaming Han, Jian Ding, Nan Xue, and Gui-Song Xia. Redet: A rotation-equivariant detector for aerial object detection. In *2021 IEEE/CVF Conference on Computer Vision and Pattern Recognition (CVPR)*, pages 2785–2794, 2021.
 - [34] Chengqi Lyu, Wenwei Zhang, Haiyan Huang, Yue Zhou, Yudong Wang, Yanyi Liu, Shilong Zhang, and Kai Chen. Rtmddet: An empirical study of designing real-time object detectors, 2022.
 - [35] Xue Yang, Gefan Zhang, Wentong Li, Xuehui Wang, Yue Zhou, and Junchi Yan. H2rbox: Horizontal box annotation is all you need for oriented object detection. *arXiv preprint arXiv:2210.06742*, 2022.
 - [36] Joseph Redmon, Santosh Divvala, Ross Girshick, and Ali Farhadi. You only look once: Unified, real-time object detection. 06 2015.
 - [37] J. Yu, Y. Jiang, Z. Wang, Z. Cao, and T. Huang. Unitbox: An advanced object detection network. *ACM*, 2016.
 - [38] Lachlan Tytsen-Smith and Lars Petersson. Improving object localization with fitness nms and bounded iou loss. In *Proceedings of the IEEE conference on computer vision and pattern recognition*, pages 6877–6885, 2018.
 - [39] H. Rezaatofghi, N. Tsoi, J. Y. Gwak, A. Sadeghian, and S. Savarese. Generalized intersection over union: A metric and a loss for bounding box regression. In *2019 IEEE/CVF Conference on Computer Vision and Pattern Recognition (CVPR)*, 2019.
 - [40] Zhaohui Zheng, Ping Wang, Wei Liu, Jinze Li, Rongguang Ye, and Dongwei Ren. Distance-iou loss: Faster and better learning for bounding box regression. In *Proceedings of the AAAI conference on artificial intelligence*, volume 34, pages 12993–13000, 2020.
 - [41] Yi-Fan Zhang, Weiqiang Ren, Zhang Zhang, Zhen Jia, Liang Wang, and Tieniu Tan. Focal and efficient iou loss for accurate bounding box regression. *Neurocomputing*, 506:146–157, 2022.
 - [42] Zhiming Chen, Kean Chen, Weiyao Lin, John See, Hui Yu, Yan Ke, and Cong Yang. Piou loss: Towards accurate oriented object detection in complex environments. In Andrea Vedaldi, Horst Bischof, Thomas Brox, and Jan-Michael Frahm, editors, *Computer Vision – ECCV*

- 2020, pages 195–211, Cham, 2020. Springer International Publishing.
- [43] Xue Yang, Junchi Yan, Qi Ming, Wentao Wang, Xiaopeng Zhang, and Qi Tian. Rethinking rotated object detection with gaussian wasserstein distance loss. In *International Conference on Machine Learning*, 2021.
- [44] Xue Yang, Xiaojiang Yang, Jirui Yang, Qi Ming, Wentao Wang, Qi Tian, and Junchi Yan. Learning high-precision bounding box for rotated object detection via kullback-leibler divergence. In M. Ranzato, A. Beygelzimer, Y. Dauphin, P.S. Liang, and J. Wortman Vaughan, editors, *Advances in Neural Information Processing Systems*, volume 34, pages 18381–18394. Curran Associates, Inc., 2021.
- [45] Xue Yang, Yue Zhou, Gefan Zhang, Jirui Yang, Wentao Wang, Junchi Yan, Xiaopeng Zhang, and Qi Tian. The kfiou loss for rotated object detection, 2022.
- [46] P. J. Huber. Robust estimation of a location parameter. *Springer New York*, 1992.
- [47] Seung-Hwan Bae. Object detection based on region decomposition and assembly. In *Proceedings of the AAAI Conference on Artificial Intelligence*, volume 33, pages 8094–8101, 2019.
- [48] Garrick Brazil, Xi Yin, and Xiaoming Liu. Illuminating pedestrians via simultaneous detection & segmentation. In *Proceedings of the IEEE International Conference on Computer Vision*, pages 4950–4959, 2017.
- [49] Chengju Zhou, Meiqing Wu, and Siew-Kei Lam. Ssa-cnn: Semantic self-attention cnn for pedestrian detection. *arXiv preprint arXiv:1902.09080*, 2019.
- [50] Mingxin Huang, Yuliang Liu, Zhenghao Peng, Chongyu Liu, Dahua Lin, Shenggao Zhu, Nicholas Yuan, Kai Ding, and Lianwen Jin. Swintextspotter: Scene text spotting via better synergy between text detection and text recognition. In *Proceedings of the IEEE/CVF Conference on Computer Vision and Pattern Recognition*, pages 4593–4603, 2022.
- [51] Pengyuan Lyu, Minghui Liao, Cong Yao, Wenhao Wu, and Xiang Bai. Mask textspotter: An end-to-end trainable neural network for spotting text with arbitrary shapes. In *Proceedings of the European Conference on Computer Vision (ECCV)*, pages 67–83, 2018.
- [52] Yin Zhou and Oncel Tuzel. Voxelnet: End-to-end learning for point cloud based 3d object detection. In *Proceedings of the IEEE conference on computer vision and pattern recognition*, pages 4490–4499, 2018.
- [53] Shaoshuai Shi, Xiaogang Wang, and Hongsheng Li. Pointcnn: 3d object proposal generation and detection from point cloud. In *2019 IEEE/CVF Conference on Computer Vision and Pattern Recognition (CVPR)*, pages 770–779. IEEE, 2019.
- [54] Ke Sun, Bin Xiao, Dong Liu, and Jingdong Wang. Deep high-resolution representation learning for human pose estimation. In *Proceedings of the IEEE/CVF conference on computer vision and pattern recognition*, pages 5693–5703, 2019.
- [55] Karim Isakov, Egor Burkov, Victor Lempitsky, and Yury Malkov. Learnable triangulation of human pose. In *Proceedings of the IEEE/CVF International Conference on Computer Vision*, pages 7718–7727, 2019.
- [56] Xinlei Chen, Ross Girshick, Kaiming He, and Piotr Dollár. Tensor-mask: A foundation for dense object segmentation. In *Proceedings of the IEEE/CVF international conference on computer vision*, pages 2061–2069, 2019.
- [57] Daniel Bolya, Chong Zhou, Fanyi Xiao, and Yong Jae Lee. Yolact: Real-time instance segmentation. In *Proceedings of the IEEE/CVF International Conference on Computer Vision (ICCV)*, October 2019.
- [58] Jiahui Yu, Yuning Jiang, Zhangyang Wang, Zhimin Cao, and Thomas Huang. Unitbox: An advanced object detection network. In *Proceedings of the 24th ACM international conference on Multimedia*, pages 516–520, 2016.
- [59] A. Paszke, S. Gross, S. Chintala, G. Chanan, E. Yang, Z. Devito, Z. Lin, A. Desmaison, L. Antiga, and A. Lerer. Automatic differentiation in pytorch. 2017.
- [60] Haoran Wei, Yue Zhang, Zhonghan Chang, Hao Li, Hongqi Wang, and Xian Sun. Oriented objects as pairs of middle lines. *ISPRS Journal of Photogrammetry and Remote Sensing*, 169:268–279, 2020.
- [61] Lin Zhou, Haoran Wei, Hao Li, Wenzhe Zhao, Yi Zhang, and Yue Zhang. Objects detection for remote sensing images based on polar coordinates, 2020.
- [62] Jingru Yi, Pengxiang Wu, Bo Liu, Qiaoying Huang, Hui Qu, and Dimitris Metaxas. Oriented object detection in aerial images with box boundary-aware vectors. In *Proceedings of the IEEE/CVF Winter Conference on Applications of Computer Vision*, pages 2150–2159, 2021.
- [63] Xue Yang, Liping Hou, Yue Zhou, Wentao Wang, and Junchi Yan. Dense label encoding for boundary discontinuity free rotation detection. In *2021 IEEE/CVF Conference on Computer Vision and Pattern Recognition (CVPR)*, pages 15814–15824, 2021.
- [64] Pengbo Zhao, Zhenshen Qu, Yingjia Bu, Wenming Tan, and Qiuyu Guan. Polardet: a fast, more precise detector for rotated target in aerial images. *International Journal of Remote Sensing*, 42(15):5831–5861, 2021.
- [65] Qi Ming, Lingjuan Miao, Zhiqiang Zhou, and Yunpeng Dong. Cfcnet: A critical feature capturing network for arbitrary-oriented object detection in remote-sensing images. *IEEE Transactions on Geoscience and Remote Sensing*, 60:1–14, 2022.
- [66] Zonghao Guo, Xiaosong Zhang, Chang Liu, Xiangyang Ji, Jianbin Jiao, and Qixiang Ye. Convex-hull feature adaptation for oriented and densely packed object detection. *IEEE Transactions on Circuits and Systems for Video Technology*, 32(8):5252–5265, 2022.
- [67] Qi Ming, Lingjuan Miao, Zhiqiang Zhou, Xue Yang, and Yunpeng Dong. Optimization for arbitrary-oriented object detection via representation invariance loss. *IEEE Geoscience and Remote Sensing Letters*, 19:1–5, 2022.
- [68] Jinwang Wang, Wen Yang, Heng-Chao Li, Haijian Zhang, and Gui-Song Xia. Learning center probability map for detecting objects in aerial images. *IEEE Transactions on Geoscience and Remote Sensing*, 59(5):4307–4323, 2021.
- [69] Xue Yang and Junchi Yan. Arbitrary-oriented object detection with circular smooth label. In Andrea Vedaldi, Horst Bischof, Thomas Brox, and Jan-Michael Frahm, editors, *Computer Vision – ECCV 2020*, pages 677–694, Cham, 2020. Springer International Publishing.
- [70] Wen Qian, Xue Yang, Silong Peng, Xiujuan Zhang, and Junchi Yan. Rsdet++: Point-based modulated loss for more accurate rotated object detection. *IEEE Transactions on Circuits and Systems for Video Technology*, 32(11):7869–7879, 2022.
- [71] Xue Yang, Junchi Yan, Wenlong Liao, Xiaokang Yang, Jin Tang, and Tao He. Srdet++: Detecting small, cluttered and rotated objects via instance-level feature denoising and rotation loss smoothing. *IEEE Transactions on Pattern Analysis and Machine Intelligence*, 45(2):2384–2399, 2023.
- [72] Xingxing Xie, Gong Cheng, Jiabao Wang, Xiwen Yao, and Junwei Han. Oriented r-cnn for object detection. In *2021 IEEE/CVF International Conference on Computer Vision (ICCV)*, pages 3500–3509, 2021.



Siliang Ma is a Ph.D student at the School of Computer Science and Engineering at South China University of Technology. He received his B.E. degree from South China Agricultural University in 2019. He is the President of CCF South China University of Technology Student Chapter. His research interests include deep learning, pattern recognition, and text image processing.



Yong Xu received the B.S., M.S., and Ph.D. degrees in mathematics from Nanjing University, Nanjing, China, in 1993, 1996, and 1999, respectively. He was a Postdoctoral Research Fellow of computer science with the South China University of Technology, Guangzhou, China, from 1999 to 2001, where he

became a Faculty Member and is currently a Professor with the School of Computer Science and Engineering. He is the vice president of South China University of Technology and the Dean of Guangdong Big Data Analysis and Processing Engineering & Technology Research Center. He is also a member of the Peng Cheng Laboratory. His current research interests include computer vision, pattern recognition, image processing, and big data. He is a senior member of the IEEE Computer Society and the ACM. He has received the New Century Excellent Talent Program of MOE Award.